Antiulcer Agents. 6. Analysis of the in Vitro Biochemical and in Vivo Gastric Antisecretory Activity of Substituted Imidazo[1,2-*a*]pyridines and Related Analogues Using Comparative Molecular Field Analysis and Hypothetical Active Site Lattice Methodologies

James J. Kaminski*,† and Arthur M. Doweyko‡

Schering-Plough Research Institute, Kenilworth, New Jersey 07033

Received September 25, 1995⊗

A number of substituted imidazo[1,2-*a*]pyridines and related analogues were selected for analysis of their in vitro biochemical and in vivo gastric antisecretory activity using comparative molecular field analysis (CoMFA) and hypothetical active site lattice (HASL) methodologies. The training set of compounds selected included those that were also chosen for an extensive molecular modeling study initiated, using the active analog approach, to define the pharmacophore by means of which **1** and its analogues interact with the gastric proton pump enzyme, H^+/K^+-ATPase. Using either CoMFA or HASL, it was possible to identify an optimal alignment paradigm of the proposed bioactive conformation for this series to reasonably predict the in vitro H^+/K^+-ATPase inhibitory potency in the purified enzyme model and the in vivo intravenous gastric antisecretory activity for compounds outside of the training set. Furthermore, the steric and electrostatic effects suggested by these two independent methods and their influence on determining biological activity were consistent and complementary to each other.

The structure−activity[1,2] relationship studies of a series of substituted imidazo[1,2-*a*]pyridines and related analogues which culminated with the identification and clinical advancement of 3-(cyanomethyl)-2-methyl-8-(phenylmethoxy)imidazo[1,2-*a*]pyridine, Sch 28080 (**1**), as an antiulcer agent exhibiting both gastric antisecretory and cytoprotective properties have been reported. In addition, an extensive investigation initiated to define the interrelationship between structure, antiulcer activity, and toxicology data[3] derived from a series of compounds chosen from our structure−activity studies to identify a successor to **1** has also been described.

Definition of the interrelationship between the conformational characteristics of this series and their antiulcer activity, examined using a variety of experimental and theoretical methods, has led to the synthesis of rigid analogues which suggested a bioactive conformation for **1**.[4] Furthermore, it has been demonstrated recently that **1**, the prototype of this series, exerts its gastric antisecretory activity in vitro, in its protonated form, by a kinetically competitive and reversible inhibition mechanism with respect to potassium ion in the extracellular domain of the gastric proton pump enzyme, H^+/K^+-ATPase.[5]

The observations described above prompted us to select a number of substituted imidazo[1,2-*a*]pyridines and related analogues from this series for biochemical characterization, in vitro, in the purified gastric proton pump enzyme, H^+/K^+-ATPase, and in the isolated intact gastric gland preparation. The inhibitory activity of these compounds determined in these two in vitro models could then be examined for correlation with their gastric antisecretory potency determined in vivo, using the histamine-stimulated Heidenhain pouch dog, following either intravenous or oral administration.

Analysis of the biological data[6] suggested that the inhibitory activity of the analogues determined in the two in vitro models is predictive of their in vivo gastric antisecretory activity following intravenous, but not oral, administration. In addition, the good correlation observed between the in vitro and in vivo models suggests that these compounds are gastric proton pump inhibitors in vivo.

A molecular modeling study[6] of these compounds using the active analog approach has defined the molecular volume which is shared by the active analogues, as well as the molecular volume which is common to the inactive analogues. Graphical representation of the difference between these molecular volumes was interpreted in terms of a hypothetical description of the pharmacophore by means of which **1** and its analogues interact with the gastric proton pump enzyme, H^+/K^+-ATPase.

With the completion of these studies, we became aware of comparative molecular field analysis (CoMFA)[7,8] and, more recently, hypothetical active site lattice (HASL)[9−12] as two promising new methodologies to structure−activity correlation. Using a select group of substituted imidazo[1,2-*a*]pyridines and related analogues, CoMFA and HASL analyses of their in vitro biochemical and/or in vivo gastric antisecretory activity were investigated.

The results of our CoMFA and HASL analyses using these selected compounds and comparison of these results with our empirically derived structure−activity relationships for this series of compounds, Figure 1, constitute the subject matter of this report.

Chemistry

The syntheses of several of the compounds investigated in this report (Table 1) have been described previously: **1**−**5** and **17**;[1] **6**, **9**, **10**, **13**, and **21**;[2] **16**;[3] and **7**, **8**, **11**, **12**, **14**, and **15**.[4] Using methodology that has been published previously,[1,2] the syntheses of **18**, **19**, and **20** are described in the Experimental Section.

* Author to whom correspondence should be addressed.
† Structural Chemistry/Computer Assisted Drug Design Department.
‡ Drug Metabolism and Pharmacokinetics Department.
⊗ Abstract published in *Advance ACS Abstracts,* January 15, 1997.

S0022-2623(95)00700-X CCC: $14.00

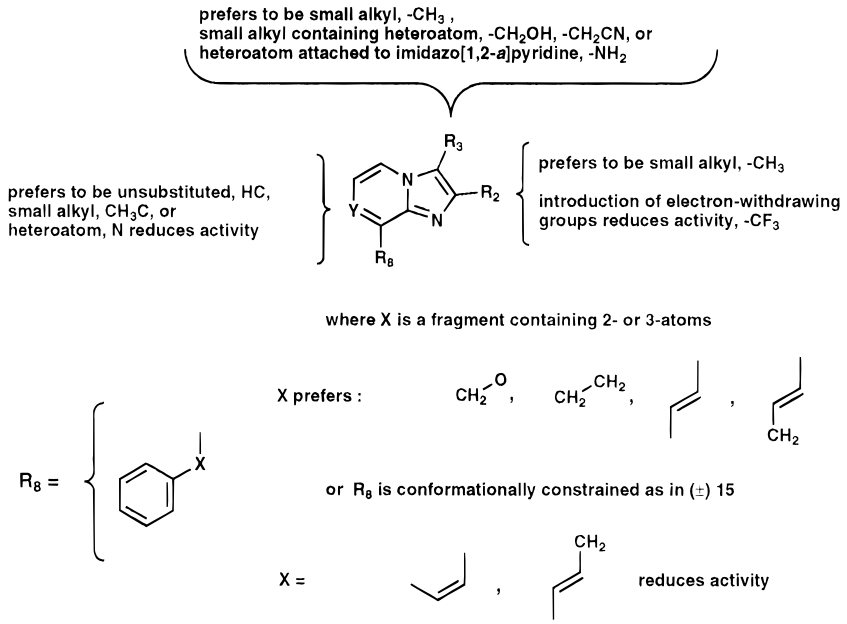

Figure 1. Selected summary of empirically derived structure−activity relationships for substituted imidazo[1,2-*a*]pyridines and related analogues based on their in vitro biochemical and in vivo gastric antisecretory activity.

Table 1. Substituted Imidazo[1,2-*a*]pyridines and Related Analogues

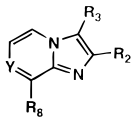

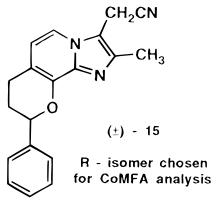

compd	Y	R_2	R_3	R_8
1	HC	CH_3	CH_2CN	$PhCH_2O$
2	HC	CH_3	CH_2OH	$PhCH_2O$
3	HC	CF_3	CH_2OH	$PhCH_2O$
4	HC	CH_3	CH_2CN	$PhCH_2CH_2$
5	HC	CF_3	CH_2CN	$PhCH_2O$
6	HC	CH_3	NH_2	$PhCH_2O$
7	HC	CH_3	CH_2CN	(*E*)-$PhCH_2CH$=CH
8	HC	CH_3	CH_2CN	(*E*)-PhCH=$CHCH_2$
9	CH_3C	CH_3	CH_2CN	$PhCH_2O$
10	HC	CH_3	NH_2	$PhCH_2CH_2$
11	HC	CH_3	NH_2	(*E*)-$PhCH_2CH$=CH
12	HC	CH_3	CH_3	(*E*)-PhCH=CH
13	N	CH_3	NH_2	$PhCH_2O$
14	HC	CH_3	CH_3	(*Z*)-PhCH=CH
15				
16	HC	CH_2CN	CH_3	$PhCH_2O$
17	HC	CH_3	CH_3	$PhCH_2O$
18	HC	CH_3	CH_3	$PhCH_2CH_2$
19	N	CH_3	CH_3	$PhCH_2O$
20	HC	CF_3	CH_3	$PhCH_2O$
21	N	CH_3	NH_2	$PhCH_2CH_2$

Biological Test Methods

Biochemical Activity. (A) Inhibition of Purified H^+/K^+-ATPase. The compounds were evaluated for their ability to inhibit purified H^+/K^+-ATPase at pH 7.4 (Table 2) using gastric membrane vesicles prepared from hog stomach by differential and zonal density gradient centrifugation as previously reported.[13] The ATPase activity was estimated as release of inorganic phosphate from ATP using the method described by LeBel et al.[14]

(B) Inhibition of H^+/K^+-ATPase in Gastric Glands. The compounds were evaluated for their ability to inhibit acid formation in rabbit gastric glands (Table 2) as described previously.[15] Histamine−stimulated acid formation in the glands was monitored by uptake of the weak base aminopyrine.

The IC_{50} values are defined as the drug concentration that gives 50% inhibition of K^+-stimulated enzyme activity, or the drug concentration that gives 50% inhibition of the maximum stimulated aminopyrine accumulation. The IC_{50} values were calculated by linear regression analysis and are expressed as IC_{50} value ± standard error of the mean.

Protein was determined according to the method described by Bradford[16] using gammaglobulin as standard.

Gastric Antisecretory Activity. The compounds were evaluated for gastric antisecretory activity (Table 2) by measuring their ability to inhibit histamine-stimulated gastric acid secretion in adult mongrel dogs with surgically prepared Heidenhain pouches as described previously.[1]

Compounds were administered intravenously (iv), 0.1−5 mg/kg and orally (po), 2−8 mg/kg. The reduction in acid output relative to the non-drug-treated control value in the same animal was measured. The dose inhibiting histamine-stimulated gastric acid secretion by 50% (ED_{50}) was calculated by linear regression analysis. The range in parentheses indicates the confidence limits of the value determined at 95%.

Computational Methods

Comparative molecular field analysis (CoMFA) of the in vitro biochemical and in vivo gastric antisecretory activity (Table 2) for the compounds described in Table 1 was carried out using the QSAR module in SYBYL Versions 5.41 and 6.1a.[18]

HASL (hypothetical active site lattice) analysis of the in vitro biochemical activities, expressed as $p^{corr}IC_{50}$, was carried out using HASL Version 3.29.[20] SYBYL cartesian coordinate files (*.mol2) were reformatted to Alchemy files (*.alc) using ConSystant Version 2.01[21] and utilized directly by the HASL program. H-value parameters, which reflect three atom types (electron-rich, electron-poor, and electron-neutral), were defined as previously reported.[9]

Table 2. In Vitro Biochemical and in Vivo Gastric Antisecretory Activity of Substituted Imidazo[1,2-*a*]pyridines and Related Analogues

	in vitro[a] biochemical activity				in vivo[b] gastric antisecretory activity		p*X* values[c]				
compd	purified H^+/K^+-ATPase IC_{50}, μmol/L	pK_a	purified H^+/K^+-ATPase $^{corr}IC_{50}$, μmol/L	gastric gland H^+/K^+-ATPase IC_{50}, μmol/L	ED_{50}^{iv}, mg/kg, $\rho = 0.05$	ED_{50}^{po}, mg/kg, $\rho = 0.05$	pIC_{50} H^+/K^+-ATPase	$p^{corr}IC_{50}$ H^+/K^+-ATPase	pIC_{50} glands	pED_{50} iv	pED_{50} po
1	1.59 ± 0.4	5.5	0.0200	0.065 ± 0.012	0.09 (0.01−1.19)	4.4 (2.1−14.0)	+5.80	+7.70	+7.19	+6.49	+4.80
2	2.2 ± 0.2	6.1[d]	0.0266	0.53 ± 0.42	0.3 (approximate)	inactive[e]	+5.65	+7.58	+6.28	+5.92	+3.00
3	inactive[e]	2[d]	0.0040	inactive[e]	inactive[e]	inactive[e]	+3.00	+8.40	+3.00	+3.00	+3.00
4	2.0 ± 0.7	6.0	0.0770	0.13 ± 0.032	0.1 (approximate)	>4.4 (approximate)	+5.70	+7.11	+6.89	+6.44	+5.17
5	inactive[e]	2[f]	0.0040	inactive[e]	inactive[e]	inactive[e]	+3.00	+8.40	+3.00	+3.00	+3.00
6	0.89 ± 0.066	6.81	0.1819	0.31 ± 0.13	0.1 (0.01−1.19)	2.0 (approximate)	+6.05	+6.74	+6.51	+6.41	+5.10
7	14 ± 0.67	5.70	0.2700	3.8 ± 1.2	1.0 (approximate)	4.0 (approximate)	+4.85	+6.57	+5.82	+5.46	+4.86
8	206 ± 36	6.0	7.9000	442 ± 23	inactive[e]	inactive[e]	+3.69	+5.10	+3.35	+3.00	+3.00
9	13.7 ± 0.73	5.67	0.2510	0.40 ± 0.16	0.53 (0.22−1.22)	7.8 (3.2−38.3)	+4.86	+6.60	+6.40	+5.74	+4.57
10	2.1 ± 0.07	7.3	0.9300	1.46 ± 0.47	1.0 (approximate)	6.7 (2.3−58.2)	+5.68	+6.03	+5.84	+5.40	+4.57
11	8.6	6.75	1.5700	14.1 ± 5.4	inactive[e]	inactive[e]	+5.07	+5.80	+4.85	+3.00	+3.00
12	1.68 ± 0.076	7.2	0.6500	0.99 ± 0.457	0.7 (0.06-2.6)	4.8 (1.6−21.5)	+5.77	+6.19	+6.00	+5.55	+4.71
13	178	4.6	0.2800	8.08	0.8 (0.2−6.0)	1.4 (0.6−3.9)	+3.70	+6.50	+5.00	+5.50	+5.26
14	28.4 ± 8.7	7.2	10.990	17.5 ± 5.3	inactive[e]	inactive[e]	+4.55	+4.96	+4.76	+3.00	+3.00
15	0.092 ± 0.021	6.0	0.0035	0.064 ± 0.002	0.06 (0.02−0.14)	3.7 (1.6−13.4)	+7.04	+8.46	+7.19	+6.70	+4.91

[a] Data obtained from ref 6. [b] Data obtained from refs 1−4. [c] Biological data expressed as p*X*, where $pX = -\log [X]$, X = biological data. [d] Data obtained from ref 5. [e] For analysis purposes, an inactive compound is arbitrarily assigned an IC_{50} or an ED_{50} value of 1000 μmol/L or 1000 μmol/kg, respectively. [f] Theoretically calculated value, ref 17.

Three-dimensional pharmacophore construction was carried out utilizing an extension of the HASL modeling procedure wherein lattice points contributing minimal information are gradually removed from the model until a small subset of significant points remain. This approach was successfully demonstrated for a series of HIV protease inhibitors.[22] In the present application, the HASL model was derived from fifteen molecules at a point - spacing of 1.50 Å. The cropping (trimming) of the HASL was conducted by: (1) removal of 2.5% of the lattice points containing partial $p^{corr}IC_{50}$ values closest to zero, (2) redistributing the partial $p^{corr}IC_{50}$ values to provide optimum activity predictions for the entire set (by minimizing the average error in activity prediction toward a target of 0.001 $p^{corr}IC_{50}$ units) and (3) repeating steps (1) and (2) until too few lattice points remain to provide meaningful activity predictions.

Results and Discussion

The substituted imidazo[1,2-*a*]pyridines and related analogues selected for CoMFA and HASL analyses included those compounds which were also chosen for an extensive molecular modeling study initiated, using the active analog approach, to define the pharmacophore by means of which **1** and its analogues interact with the gastric proton pump enzyme, H^+/K^+-ATPase.[6]

The CoMFA and HASL analyses of the in vitro biochemical and/or in vivo gastric antisecretory activity for the compounds, **1**−**15**, investigated in this study involved three distinct phases:

(a) Selection of a conformation for each of the substituted imidazo[1,2-*a*]pyridines and related analogues to be used in the analyses.

(b) Evaluation and further processing of the data derived from each analysis for each of the in vitro biochemical and/or in vivo gastric antisecretory properties examined, if warranted.

(c) Prediction of the in vitro biochemical and/or the in vivo gastric antisecretory activity of substituted imidazo[1,2-*a*]pyridines and related analogues which were not used in the derivation of the CoMFA and/or HASL analysis.

A synopsis of our results in each phase of these studies is described below.

A. Selection of a Conformation for Each of the Substituted Imidazo[1,2-a]pyridines and Related Analogues Used in the CoMFA and HASL Analyses. Modeling studies using the protonated form of the compounds described above using SYBYL Version 3.4 and MacroModel V1.5[19] have been reported.[6] These studies allowed determination of the global minimum energy conformation for each of the substituted imidazo[1,2-*a*]pyridines and related analogues described in Table 1. These global minimum energy conformations were determined by carrying out conformational searches within SYBYL. The valid conformations obtained from each search were then individually minimized using the MM2 force field in MacroModel applying the block diagonal Newton−Raphson algorithm. The minimum energy conformation and those conformations within 20 kJ/mol (∼5 kcal/mol) of the minimum energy conformation were recorded.

It should be noted that the conformational searches described above were conducted with and without distance constraints defined for the phenyl group in each of the substituted imidazo[1,2-*a*]pyridines and related analogues investigated. The distance constraints were determined from the position of the phenyl group in the most potent, in vitro and in vivo, and constrained compound, **15**. It was found that for active compounds there was no significant energetic cost associated with the phenyl groups' adopting the conformation of the phenyl group of **15**, while for inactive compound **14**, the energetic cost was 6.95 kJ/mol, 1.7 kcal/mol. On the basis of these results, the global minimum energy conformation of **15**, which contains the phenyl group in a pseudoequatorial conformation, was proposed to mimic the bioactive conformation for this series.

Therefore, in addition to using the global minimum energy conformation of each of the substituted imidazo[1,2-*a*]pyridines and related analogues as the relevant conformation in the analysis, the proposed bioactive conformation of **15** could also be used as a template from which to construct another possibly relevant conformation for each of the other substituted imidazo[1,2-*a*]pyridines and related analogues. Regardless of which conformation is chosen for the CoMFA and HASL analyses, partial atomic charges associated with each

Table 3. Comparative Molecular Field Analyses (CoMFA) of the in Vitro Biochemical and in Vivo Gastric Antisecretory Activity of Substituted Imidazo[1,2-*a*]pyridines and Related Analogues Using Their Global Minimum Energy and Template-based Conformations

In Vitro Biochemical Activity						
	purified H^+/K^+-ATPase plC_{50} database		purified H^+/K^+-ATPase $p^{corr}IC_{50}$ database		gastric gland H^+/K^+-ATPase plC_{50}^{gland} database	
CoMFA parameter	A[a]	B[b]	A[a]	B[b]	A[a]	B[b]
cross-validation	15	15	15	15	15	15
components	5	5	5	5	5	5
cross-validated r^2	−0.693	−0.220	+0.398	+0.402	+0.164	+0.292
standard error of prediction	+1.594	+1.542	+1.091	+0.984	+1.638	+1.430
optimum number of components	1	4	5	3	5	4
F value	0	0	1.2	1.2	0.4	0.7

In Vivo Gastric Antisecretory Activity				
	pED_{50}^{iv} database		pED_{50}^{po} database	
CoMFA parameter	A[a]	B[b]	A[a]	B[b]
cross-validation	15	15	15	15
components	5	5	5	5
cross-validated r^2	+0.203	+0.401	−0.177	−0.236
standard error of prediction	+1.670	+1.373	+1.192	+1.124
optimum number of components	5	4	3	1
F value	0.5	1.2	0	0

[a] Database A contains the global minimum energy conformations of the substituted imidazo[1,2-*a*]pyridines and related analogues used in the CoMFA analysis. [b] Database B contains the template-based conformations of the substituted imidazo[1,2-*a*]pyridines and related analogues used in the CoMFA analysis.

conformation were calculated using the AM 1 molecular orbital approximation method.

Finally, the global minimum energy conformation and the template-based conformation of each substituted imidazo[1,2-*a*]pyridine and related analogue was compared to the global minimum energy conformation of **15** by fitting the atoms of the imidazo[1,2-*a*]pyridine ring system using the FIT command within SYBYL. The compared conformers and their associated partial atomic charges were individually stored in databases A and B, Table 3, respectively.

B. Evaluation and Further Processing of the Data Derived from Comparative Molecular Field Analysis of the in vitro Biochemical and in vivo Gastric Antisecretory Activity of Substituted Imidazo[1,2-a]pyridines and Related Analogues. In general, comparative molecular field analysis (CoMFA) of any molecular property, physical or biological, using partial least squares (PLS) methodology which exhibits a cross-validated r^2 value (q^2) $\geq$ 0.3 suggests that the probability of a "correlation by chance" between the property and the CoMFA field examined is approximately $\leq$5%.[23]

In light of this suggestion, comparative molecular field analysis of the in vitro biochemical and the in vivo gastric antisecretory activity of the substituted imidazo-[1,2-*a*]pyridines and related analogues, **1**−**15**, described in Table 1 using their global minimum energy and their template-based conformations are summarized in Table 3.

Evaluation of the results of these studies suggests the following.

1. A poor comparative molecular field analysis is obtained for the inhibitory potency of the compounds in the in vitro purified enzyme model determined at pH 7.4 using either their global minimum energy or their template-based conformations, *i.e.*, cross-validated $r^2 < 0$, *F* value = 0.

However, since it has been established that the prototype of this series, **1**, exerts its inhibitory effect in vitro in its protonated form, a better comparative molecular field analysis is obtained when correction is made for the percentage of compound existing in its protonated form at pH 7.4, *i.e.*, cross-validated r^2 = +0.398, *F* value = 1.2, and cross-validated r^2 = +0.402, *F* value = 1.2, using the global minimum energy and template-based conformations, respectively.

The fraction of compound protonated at the solution pH of the purified enzyme assay can be determined from the relationship, $[ImPH^+]/[ImP] = 10^{-(pH-pK_a)} = 10^{-(7.4-pK_a)}$, where $[ImPH^+]$ refers to the concentration of the protonated form of the substituted imidazo[1,2-*a*]pyridine or related analogue, and [ImP] refers to its concentration in the unprotonated form.

Comparative molecular field analysis of the inhibitory potency of these compounds in the intact gastric gland preparation is not as good as that obtained from the in vitro purified enzyme model when correction is made for the percentage of compound existing in its protonated form, *i.e*, cross-validated r^2 = +0.292, *F* value = 0.7.

In all the instances described above, marginally better cross-validated r^2 and *F* values were obtained from the comparative molecular field analysis of the in vitro biochemical activity when the template-based conformations were used, rather than the global minimum energy conformations.

2. Comparative molecular field analysis of the in vivo oral potency of substituted imidazo[1,2-*a*]pyridines and related analogues to inhibit gastric acid secretion is also poor, *i.e.*, cross-validated $r^2 < 0$, *F* value = 0, while the cross-validated r^2 values obtained from comparative molecular field analysis of their intravenous potency to inhibit gastric acid secretion is +0.203, *F* value = 0.5 and +0.401, *F* value = 1.2, using the global minimum energy and template-based conformations, respectively.

Once again, in all the cases examined, marginally better cross-validated r^2 and *F* values were obtained from comparative molecular field analysis of the in vivo gastric antisecretory activity when the template-based conformations were used, rather than the global minimum energy conformations.

The significant cross-validated r^2 values obtained from the comparative molecular field analyses described

above for the in vitro biochemical and in vivo gastric antisecretory activity of the substituted imidazo[1,2-*a*]-pyridines and related analogues, **1**−**15**, are in qualitative agreement with the correlations also observed by graphical analysis of these in vitro and in vivo biological data expressed as pX, where pX = −log [X], X = biological data, which have been reported previously.[6]

While new approaches to improve the results obtained from comparative molecular field analyses have recently been reported,[24,25] we investigated a user-independent method for "fitting" the global minimum energy and template-based conformations of **1**−**15** and its concomitant effect on the cross-validated r^2 values obtained from comparative molecular field analysis of the in vitro biochemical and in vivo gastric antisecretory activity of the substituted imidazo[1,2-*a*]pyridines and related analogues.

A steric and electrostatic alignment program was obtained[26] and adapted to run in the UNIX environment. The program optimizes the alignment of two three-dimensional structures with each other using their steric volumes, and/or their electrostatic potential fields as factors. Initially, the effect of aligning the steric volumes, and the electrostatic potential fields of each of the substituted imidazo[1,2-*a*]pyridines and related analogues, **1**−**15**, on the cross-validated r^2 value obtained from comparative molecular field analysis of the in vitro purified enzyme model (corrected for the percentage of compound existing in its protonated form) was independently examined under a variety of fitting paradigms using both the global minimum energy and template-based conformations. In each case, alignment of the steric volumes, or electrostatic potential fields were fit to the most potent, in vitro and in vivo, and constrained analogue, **15**, as the fixed reference molecule. The results of these studies are summarized in Table 4.

Regardless of the conformation chosen, *i.e.*, the global minimum energy conformation versus the template-based conformation, alignment of the electrostatic potential field had a greater effect on the value of the cross-validated r^2 observed relative to alignment of the steric volume. When various permutations and combinations in proportion of steric and electrostatic alignments were examined, the highest cross-validated r^2 value was observed when the substituted imidazo[1,2-*a*]pyridines and related analogues were sterically (25%) and electrostatically (75%) aligned using either the global minimum energy conformation or the template-based conformation. Interestingly, the cross-validated r^2 and F values obtained using the global minimum energy conformation, cross-validated r^2 = +0.688, F value = 4.0, were marginally greater than those observed when using the template-based conformation, cross-validated r^2 = +0.535, F value = 2.1, which was proposed to mimic the relevant, bioactive conformation.

Subsequently, using only the template-based conformations, the effect of aligning the steric volumes, and the electrostatic potential fields of each of the substituted imidazo[1,2-*a*]pyridines and related analogues, **1**−**15**, on the cross-validated r^2 and F values obtained from comparative molecular field analysis of the in vitro gastric gland activity and the in vivo intravenous gastric antisecretory activity under a variety of fitting paradigms were also examined. Once again, alignment of the steric volumes, or electrostatic potential fields

Table 4. Comparative Molecular Field Analyses (CoMFA) of the In vitro Purified H^+/K^+-ATPase Activity ($p^{corr}IC_{50}$) for Substituted Imidazo[1,2-*a*]pyridines and Related Analogues, 1−15, Using their Global Minimum Energy and Template-based Conformations, Database A and B

	database A: global minimum energy conformation analysis								database B: template-based conformation analysis							
		cross-validated				conventional			cross-validated				conventional			
fitting procedure	optimum number of components	r^2	standard error of prediction	F value	composition St/El (%)	r^2	standard error of estimate	optimum number of components	r^2	standard error of prediction	F value	composition St/El (%)	r^2	standard error of estimate
−[a,b]	5	+0.398	+1.091	1.2	81/19	+0.993	+0.114	3	+0.402	+0.984	1.2	85/15	+0.864	+0.469
electrostatic (El)	5	+0.615	+0.873	2.9	76/24	+0.996	+0.090	5	+0.508	+0.987	1.9	79/21	+0.975	+0.223
steric (St)	5	+0.509	+0.985	1.9	70/30	+0.995	+0.099	5	+0.316	+1.164	0.8	76/24	+0.993	+0.115
St/El (50/50)	5	+0.257	+1.213	0.6	84/16	+0.996	+0.087	5	+0.466	+1.028	1.6	78/21	+0.969	+0.246
St/El (25/75)	5	+0.688	+0.786	4.0	74/26	+0.997	+0.082	5	+0.535	+0.960	2.1	79/21	+0.967	+0.254
St/El (75/25)	5	+0.160	+1.289	0.3	80/20	+0.998	+0.065	5	+0.337	+1.145	0.9	76/24	+0.979	+0.206

[a] The global minimum energy conformation for each substituted imidazo[1,2-*a*]pyridine or related analogue was compared to the *R* isomer of **15** by fitting the atoms of the imidazo[1,2-*a*]pyridine ring system using the FIT command within SYBYL. [b] Compound **15** was used as the template to derive the conformations of the other substituted imidazo[1,2-*a*]pyridines and related analogues. The compounds were compared to the *R* isomer of **15** by fitting the atoms of the imidazo[1,2-*a*]pyridine ring system using the FIT command within SYBYL.

were fit to the most potent, in vitro and in vivo, and constrained analogue, **15**, as the fixed reference molecule. The results of these studies are described in Table 5.

Regardless of the biologic activity examined, *i.e.*, in vitro gastric gland H^+/K^+-ATPase activity or in vivo intravenous gastric antisecretory activity, alignment of the electrostatic potential field had a greater effect on the value of the cross-validated r^2 observed relative to alignment of the steric volume. The highest cross-validated r^2 and F values were again observed when the substituted imidazo[1,2-*a*]pyridines and related analogues were sterically (25%) and electrostatically (75%) aligned. Cross-validated r^2 and F values of +0.529 and 2.0, and +0.508 and 1.9, were obtained for the in vitro gastric gland H^+/K^+-ATPase activity and the in vivo intravenous gastric antisecretory activity, respectively.

C. Prediction of the in vitro Biochemical and/or the in vivo Gastric Antisecretory Activity of Substituted Imidazo[1,2-a]pyridines and Related Analogues. The best cross-validated r^2 values were obtained from comparative molecular field analysis of the following properties: the H^+/K^+-ATPase inhibitory potency of the compounds determined in vitro in the purified enzyme model, corrected for the percentage of compound existing in its protonated form at pH 7.4, p^{corr}-IC_{50}, and the intravenous gastric antisecretory activity of the compounds determined in vivo, pED_{50}^{iv}, each using template-based conformations, *i.e.*, cross-validated $r^2 = +0.402$, F value = 1.2, and cross-validated $r^2 = +0.401$, F value = 1.2, respectively, Table 3.

Furthermore, the cross-validated r^2 values obtained for the comparative molecular field analyses of these properties could be improved when the substituted imidazo[1,2-*a*]pyridines and related analogues, **1**−**15**, using their template-based conformations, were sterically (25%) and electrostatically (75%) aligned, *i.e.*, cross-validated $r^2 = +0.535$, F value = 2.1, and cross-validated $r^2 = +0.508$, F value = 1.9, respectively. Therefore, the comparative molecular field analyses for these properties using the latter criteria were selected to predict the in vitro H^+/K^+-ATPase inhibitory potency in the purified enzyme model (corrected for the percentage of compound existing in its protonated form at pH 7.4) $p^{corr}IC_{50}$, and the in vivo intravenous gastric antisecretory activity, pED_{50}^{iv}, for analogues **16**−**21**, which were not included in the derivation of these CoMFA models. Unfortunately, $p^{corr}IC_{50}$ values for **16**−**21** were not experimentally available. However, using the following relationships a pED_{50}^{iv} could be calculated for each compound based on its CoMFA predicted $p^{corr}IC_{50}$ value:

$$\text{purified } H^+/K^+\text{-ATPase } IC_{50}\ (\mu M) = 10^{(6-p^{corr}IC_{50})}/10^{-(7.4-pK_a)}$$

$$plC_{50}\ H^+/K^+\text{-ATPase} = -\log\ [H^+/K^+\text{-ATPase } IC_{50}]$$

$$pED_{50}^{iv} = +0.973(plC_{50}\ H^+/K^+\text{-ATPase}) + 0.146$$

Using this procedure, the "calculated" pED_{50}^{iv} values based on their CoMFA-predicted $p^{corr}IC_{50}$ values and the "predicted" pED_{50}^{iv} values from the CoMFA model based on the intravenous gastric antisecretory activities of the compounds determined in vivo, each converted to their

Table 5. Comparative Molecular Field Analyses (CoMFA) of the in Vitro Gastric Gland H^+/K^+-ATPase Activity (plC_{50}^{gland}) and the in Vivo Intravenous Gastric Antisecretory Activity (pED_{50}^{iv}) for Substituted Imidazo[1,2-*a*]pyridines and Related Analogues, **1**−**15**, Using Their Template-Based Conformations, Database B

	in vitro gastric gland H^+/K^+-ATPase activity plC_{50}^{gland}							in vivo intravenous gastric antisecretory activity pED_{50}^{iv}						
		cross-validated				conventional			cross-validated				conventional	
fitting procedure	optimum number of components	r^2	standard error of prediction	F value	composition St/El (%)	r^2	standard error of estimate	optimum number of components	r^2	standard error of prediction	F value	composition St/El (%)	r^2	standard error of estimate
—[a]	4	+0.292	+1.430	0.7	65/35	+0.870	+0.614	4	+0.401	+1.373	1.2	67/33	+0.886	+0.599
electrostatic (El)	4	+0.323	+1.398	0.9	68/32	+0.899	+0.540	4	+0.490	+1.267	1.7	68/32	+0.901	+0.557
steric (St)	4	+0.222	+1.499	0.5	58/42	+0.918	+0.488	4	+0.239	+1.548	0.6	62/38	+0.947	+0.409
St/El (50/50)	5	+0.395	+1.394	1.2	66/34	+0.949	+0.403	5	+0.438	+1.402	1.4	68/32	+0.918	+0.536
St/El (25/75)	5	+0.529	+1.230	2.0	69/31	+0.964	+0.339	5	+0.508	+1.312	1.9	69/31	+0.938	+0.466
St/El (75/25)	5	+0.240	+1.562	0.6	67/33	+0.933	+0.462	5	+0.343	+1.516	0.9	68/32	+0.932	+0.487

[a] Compound **15** was used as the template to derive the conformations of the other substituted imidazo[1,2-*a*]pyridines and related analogues. The compounds were compared to the *R* isomer of **15** by fitting the atoms of the imidazo[1,2-*a*]pyridine ring system using the FIT command with SYBYL.

Table 6. Comparison between the CoMFA Predicted in Vitro Biochemical ($p^{corr}IC_{50}$) and in Vivo Intravenous Gastric Antisecretory Activity (pED_{50}^{iv}) of Substituted Imidazo[1,2-*a*]pyridines and Related Analogues, **1**−**15**, Using Their Template-Based Conformations That Were Sterically/Electrostatically Fit (25/75) to the *R* Isomer of **15**

compd	CoMFA predicted value purified H^+/K^+-ATPase $p^{corr}IC_{50}$	Calculated[a] values based on $p^{corr}IC_{50}$			CoMFA predicted value pED_{50}^{iv}	calculated[b] values based on pED_{50}^{iv} ED_{50}^{iv}, mg/kg	experimental value approximate ED_{50}^{iv}, mg/kg	estimated value based on approximate ED_{50}^{iv} purified H^+/K^+-ATPase $p^{corr}IC_{50}$
		IC_{50}, μM	pED_{50}^{iv}	ED_{50}^{iv}, mg/kg				
16[c]	7.32	3.8	5.42	1.1	4.37	11.8	0.8	7.44
17[d]	6.73	0.47	6.31	0.13	5.61	0.6	0.1	6.83
18[e]	6.31	0.39	6.38	0.11	5.38	1.1	0.2	6.02
19[f]	6.56	110	4.00	25.3	5.35	1.1	2	7.69
20[g]	7.76	4365	2.44	1112	2.72	584	inactive[i]	3.00[j]
21[h]	6.14	145	3.88	33	5.38	1.1	inactive[i]	3.00[j]

[a] Values calculated from the following relationships: Purified H^+/K^+-ATPase IC_{50} (μM) = $10^{(6-p^{corr}IC_{50})}/10^{-(7.4-pK_a)}$; $p^{corr}IC_{50} = -\log[^{corr}IC_{50}]$; $pED_{50}^{iv} = +0.973(pIC_{50}\ H^+/K^+\text{-ATPase}) + 0.146$, $r_c = +0.766$.[6] [b] Values calculated from the following relationship: $pED_{50}^{iv} = -\log [ED_{50}^{iv}]$. [c] Theoretical pK_a (**16**) = 5.5.[17] [d] Experimentally determined pK_a (**17**) = 7.0. [e] Theoretical pK_a (**18**) = 7.5.[17] [f] Theoretical pK_a (**19**) = 4.8.[17] [g] Theoretical pK_a (**20**) = 2.0.[17] [h] Theoretical pK_a (**21**) = 5.1.[17] [i] The inhibition of gastric acid secretion in the Heidenhain pouch dog was less than 20% following intravenous administration at a 5 mg/kg screening dose. [j] For analysis purposes, an inactive compound is arbitrarily assigned an ED_{50} value of 1000 μmol/kg.

corresponding ED_{50}^{iv} values, could then be compared directly to their experimentally determined "approximate" ED_{50}^{iv} values. The results of these studies are summarized in Table 6.

Comparison of the "calculated" ED_{50}^{iv} values from the CoMFA predicted $p^{corr}IC_{50}$ values, or the CoMFA "predicted" pED_{50}^{iv} values, relative to their experimentally determined "approximate" ED_{50}^{iv} values are in the worst case, predicted to within one order of magnitude, *e.g.*, **19** and **16**, and in most cases, within a 5−6-fold difference. In addition, the inactivity of **20**, predicted by either CoMFA model, is in good agreement with the lack of inhibition of gastric acid secretion observed in the Heidenhain pouch dog following intravenous administration of **20** at a 5 mg/kg screening dose. However for **21**, the gastric antisecretory activity predicted by either CoMFA model is inconsistent with its experimentally observed lack of gastric antisecretory activity.

On the basis of the CoMFA determined structure−activity relationship results, a predictive 3D pharmacophore was constructed from the $p^{corr}IC_{50}$ activities of the substituted imidazo[1,2-*a*]pyridines and related analogues, **1**−**15**, using their template-based conformations, following the HASL modeling paradigm described previously.[22] This was done by first creating a 265 point HASL description of the 15-membered training set at a resolution of 1.50 Å. A trimming process was applied to this model wherein 2.5% of the lattice points were removed at a time, targeting those contributing the least information, *i.e.*, having partial activity values nearest zero, and monitoring each resulting model for predictivity, *i.e.*, comparison of actual versus predicted activity for the training set. After 36 trimming cycles, a 15-point HASL model emerged which predicted the activity of the training set with a correlation coefficient = +0.972. Further trimming of this model led to a rapid degradation of performance, suggesting that the 15 remaining points were significant to the model. The 15-point HASL model was examined further by conducting a "leave-one-out" crossvalidation using the 15-membered training set. The results of this analysis are compared to those obtained from the comparative molecular field analysis using the same 15-membered training set, Table 7. Comparison of each of the CoMFA and HASL predicted activities to the actual activity for the 15-membered training set were found to be significant and identical, correlation coefficient = +0.539 for CoMFA predictions, and correlation coefficient = +0.853 for HASL predictions, Table 7 and Figure 2a.

Table 7. Comparison of CoMFA and HASL Predictivities

compd	actual $p^{corr}IC_{50}$	CoMFA predicted[a] $p^{corr}IC_{50}$	HASL predicted[a] $p^{corr}IC_{50}$
1	7.70	7.17	8.27
2	7.58	7.68	8.15
3	8.40	8.61	7.77
4	7.11	7.07	7.32
5	8.40	8.07	7.90
6	6.74	6.51	6.54
7	6.57	5.70	6.67
8	5.10	6.37	4.45
9	6.60	7.46	6.09
10	6.03	6.65	5.67
11	5.80	5.89	5.81
12	6.19	7.06	6.06
13	6.50	6.40	6.76
14	4.96	5.73	5.65
15	8.46	6.75	8.20
		+0.539[b]	+0.853[b]
16	7.44	7.32	6.70
17	6.83	6.73	6.55
18	6.02	6.31	6.25
19	7.69	6.56	6.36
20	3.00	7.76	7.39
21	3.00	6.14	5.95

[a] 15-membered training set predictions are based on a "leave-one-out" cross-validation analysis. [b] Correlation coefficient.

The extent to which the two methodologies could predict the activity of compounds which were not part of the training set, *e.g.*, **16**−**21**, was also examined using the same 15-point HASL model as a basis, Table 7. Graphical analysis of the CoMFA and HASL activity predictions for this set of compounds, as well as the training set, reveals a similar trend between the activity predictions made by either method, yielding correlation coefficients of +0.338 and +0.928 for the **1**−**15** and **16**−**21** compound sets, respectively (Figure 2b). This observation is indicative of an underlying similarity between the two modeling paradigms.

Identification of the steric (25%) and electrostatic (75%) alignment paradigm as optimal for this series by HASL was consistent with the results obtained from the comparative molecular field analysis of the substituted imidazo[1,2-*a*]pyridines and related analogues, **1**−**15**, Table 4. These studies also identified the steric (25%) and electrostatic (75%) alignment paradigm as optimal, and produced an analysis exhibiting a cross-validated r^2 = +0.535 and a conventional r^2 = +0.967, respectively.

Interestingly, the expression for biological activity determined from the comparative molecular field analysis using this alignment paradigm, *i.e.*, biological activ-

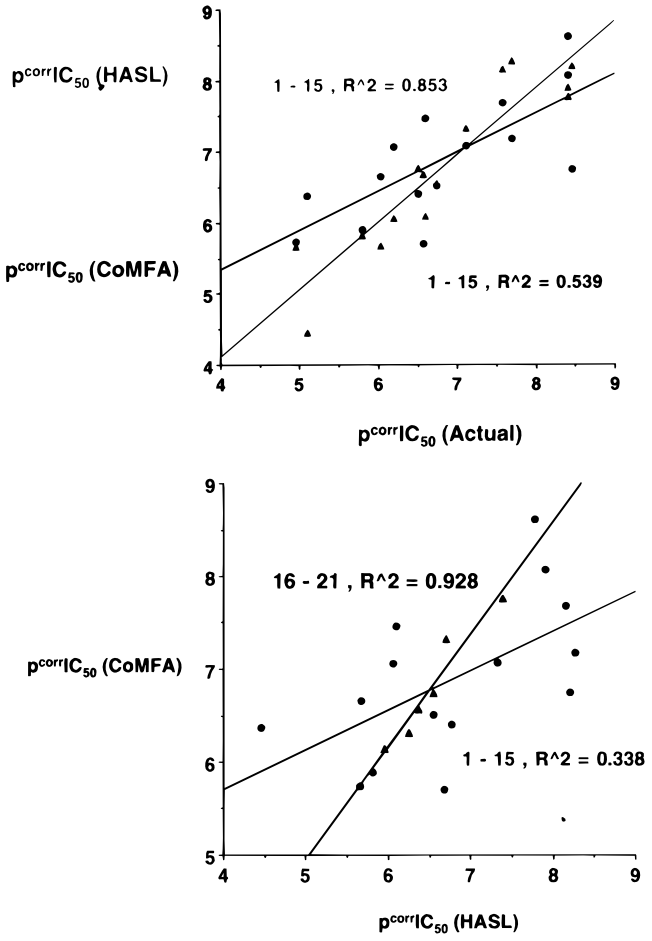

Figure 2. (a, Top) Comparison between the comparative molecular field analysis, $p^{corr}IC_{50}$ (CoMFA), and hypothetical active site lattice, $p^{corr}IC_{50}$ (HASL) activity predictions of the in vitro purified H^+/K^+-ATPase activity for substituted imidazo[1,2-*a*]pyridines and related analogues, **1**−**15**, using their template-based conformations relative to the experimentally determined in vitro purified H^+/K^+-ATPase activity, $p^{corr}IC_{50}$ (actual). (b, Bottom) Comparison between the comparative molecular field analysis (CoMFA) and hypothetical active site lattice (HASL) activity predictions of the in vitro purified H^+/K^+-ATPase activity ($p^{corr}IC_{50}$) for substituted imidazo[1,2-*a*]-pyridines and related analogues, **1**−**15** and **16**−**21**, using their template-based conformations.

ity = +1.97(steric) + 0.54(electrostatic) + intercept, emphasizes a greater contribution from the steric term (79%) to the biological activity relative to the electrostatic term (21%). The observed weighting in the expression for biological activity is dramatically opposed to the weighting of the alignment paradigm, steric (25%) and electrostatic (75%), which was identified as optimal. However, comparison of the steric and electrostatic composition for alternative alignment paradigms indicates that a greater contribution from the steric term (75 ± 5%) is consistently observed relative to the electrostatic term (20 ± 5%), Table 4. While novel methods to improve comparative molecular field analysis results have recently become available,[24,25] *e.g.*, by optimizing alignments, region focusing, maximizing cross-validation, and altering steric and electrostatic weightings, these approaches were not the objective of this study.

Descriptions of the H^+/K^+-ATPase active site binding requirements as proposed by the CoMFA and HASL models are illustrated in Figures 3 and 4, and Figures 5 and 6, respectively. These features are visualized in three-dimensional space with reference to **15**, the most

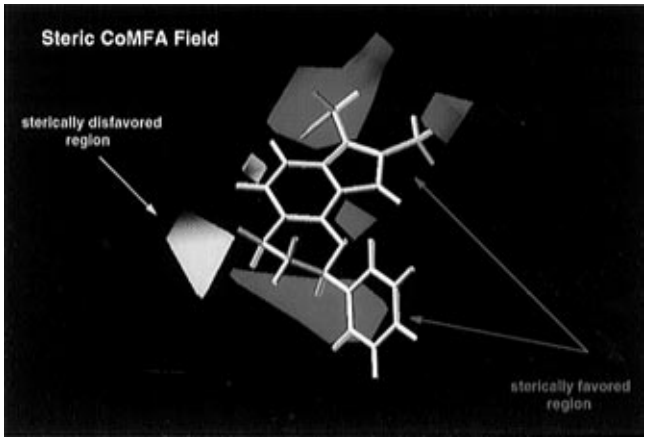

Figure 3. Steric CoMFA field from the analysis of the in vitro purified H^+/K^+-ATPase activity ($p^{corr}IC_{50}$) for substituted imidazo[1,2-*a*]pyridines and related analogues, **1**−**15**, using their template-based conformations that were sterically/electrostatically fit (25/75).

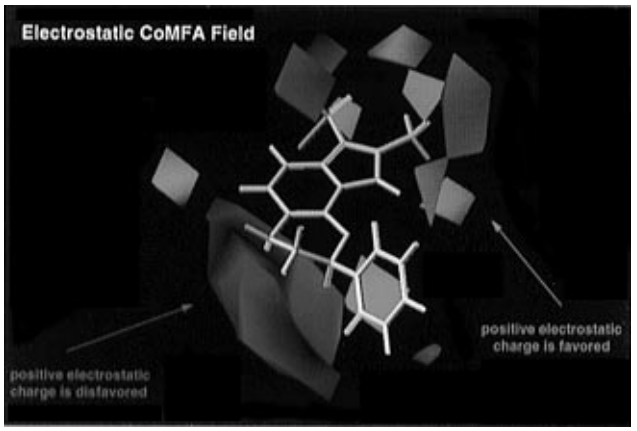

Figure 4. Electrostatic CoMFA field from the analysis of the in vitro purified H^+/K^+-ATPase activity ($p^{corr}IC_{50}$) for substituted imidazo[1,2-*a*]pyridines and related analogues, **1**−**15**, using their template-based conformations that were sterically/electrostatically fit (25/75).

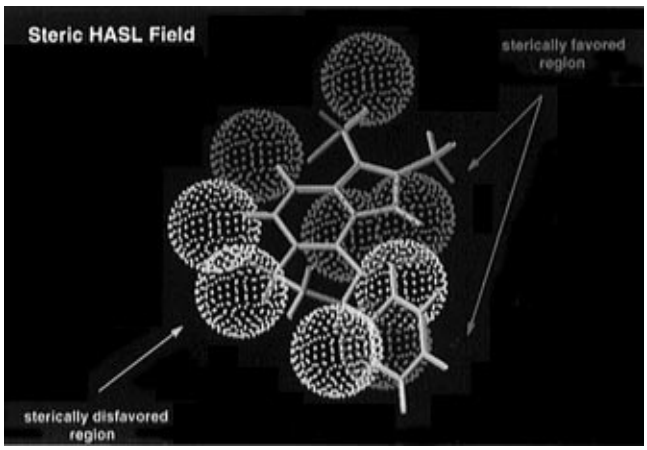

Figure 5. Steric HASL field from the analysis of the in vitro purified H^+/K^+-ATPase activity ($p^{corr}IC_{50}$) for substituted imidazo[1,2-*a*]pyridines and related analogues, **1**−**15**, using their template-based conformations that were sterically/electrostatically fit (25/75).

potent, in vitro and in vivo, and constrained analogue. The steric and electrostatic CoMFA fields are depicted separately in Figures 3 and 4. The HASL-derived 3D pharmacophore identifying regions contributing positive and negative steric effects to H^+/K^+-ATPase activity, and representing atom type information, *i.e.*, electron-

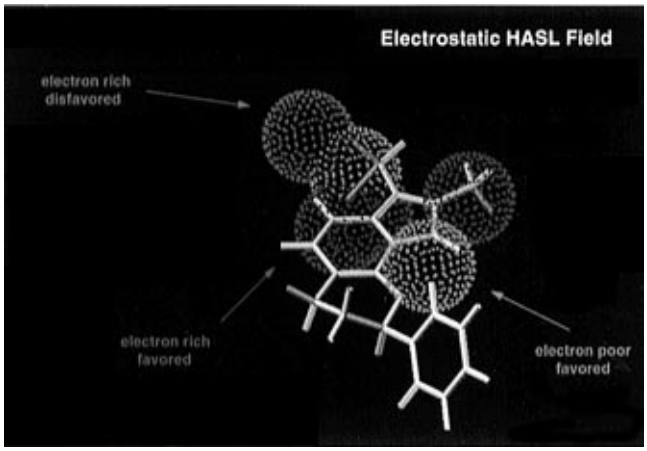

Figure 6. Electrostatic HASL field from the analysis of the in vitro purified H^+/K^+-ATPase activity ($p^{corr}IC_{50}$) for substituted imidazo[1,2-*a*]pyridines and related analogues, **1**−**15**, using their template-based conformations that were sterically/electrostatically fit (25/75).

rich, electron-neutral, and electron-poor regions, are illustrated in Figures 5 and 6.

Since the CoMFA fields are derived externally by probing outside the structure, while the HASL model reflects regions found within atoms belonging to the structure, a direct comparison of the results from these two methods might lead to some interpretive conundrums. Nevertheless, both methods are dependent upon a convergent process beginning with a previously aligned set of molecules, positioned in a regularly-spaced grid of points, ultimately identifying regions defined by these points as significant to effecting binding, *i.e.*, biological activity. Given this perspective, it is possible that the two methods could lead to similar conclusions from their individually derived active site models.

One such interpretive overlap is evident when comparing the steric effects for binding, and their concomitant effect on H^+/K^+-ATPase inhibitory activity, predicted by the CoMFA and HASL steric fields, Figures 3 and 5, respectively. The electron-neutral atom type defined in HASL can be taken as essentially equivalent to exerting a steric effect in this comparison. The HASL model contains several sterically disfavored regions (Figure 5, yellow) which closely coincide with similar regions in the steric CoMFA field (Figure 3, yellow) residing near the 7-position of the imidazo[1,2-*a*]pyridine ring system in **15**. Sterically favored regions in both models (Figures 3 and 5, green) are found near the 2-, 3-, and 8-positions of the imidazo[1,2-*a*]pyridine ring system in **15**. These 3D-QSAR findings are consistent between the two models, consistent with the active analogue pharmacophore model,[6] and reflect the steric constraints which had been empirically derived from the structure−activity relationship study directed by synthesis,[1−4] Figure 1.

Comparison between the electrostatic CoMFA field and the electrostatic HASL field defined by electron-rich and electron-poor atom types is not as straightforward as the steric field interpretation. This difference may be a consequence that electron-rich or electron-poor atom types may exert different electrostatic fields depending upon their degree of protonation. Regions where positive electrostatic charge is favored are identified in the electrostatic CoMFA field (Figure 4, cyan) near the 2-, 3-, and 8-positions of the imidazo[1,2-*a*]-pyridine ring system in **15**. In the HASL model, the imidazo[1,2-*a*]pyridine ring system is bracketted by regions favorable to activity consisting of three electron-rich (red) and two electron-poor (cyan) regions, Figure 6. Consistency between the two methods requires that the electron-rich regions reflect protonated species which in the case of the imidazo[1,2-*a*]pyridine ring system would correspond to ring protonation. The single electron-rich disfavored region (Figure 6, magenta) residing near the 3-position of the imidazo[1,2-*a*]pyridine ring system is also consistent with the CoMFA mix of favored and disfavored electrostatics near the same site. The CoMFA-identified region (Figure 4, red) near the 8-position of the imidazo[1,2-*a*]pyridine ring system in **15**, which disfavors positive electrostatic charge, is not observed in the HASL model. However, the same region was identified as sterically favored by HASL.

Such interpretive differences may originate from the contrasting approaches found in the very definitions of either model, *i.e.*, the relationship between atom type and the field effect may easily be obscured by possible degrees of protonation or solvation. That these two methods provide similar 3D-QSAR modeling insight, despite these limitations, suggests that 3D-QSAR analysis utilizing occupied molecular space and a simple set of atom type definitions can neatly complement the analysis of steric and electrostatic forces surrounding that space.

In conclusion, using either CoMFA or HASL and a limited training set of substituted imidazo[1,2-*a*]pyridines and related analogues, it was possible to identify an optimal alignment paradigm, steric (25%) and electrostatic (75%), of the proposed bioactive conformation for this series to reasonably predict the in vitro H^+/K^+-ATPase inhibitory potency in the purified enzyme model, corrected for the percentage of compound existing in its protonated form at pH 7.4, $p^{corr}IC_{50}$, and the in vivo intravenous gastric antisecretory activity, pED_{50}^{IV}, of compounds outside of the training set. Furthermore, the steric and electrostatic effects suggested by these two independent methods, and their influence on determining biological activity, were consistent and complementary to each other.

Experimental Section

Melting points were determined with a Thomas Hoover melting point apparatus and are uncorrected. The NMR spectra were recorded with a Varian CFT-20 or Varian XL-400 spectrometer, IR spectra were recorded with a Perkin-Elmer 221 spectrophotometer, and mass spectra were obtained with a Varian MAT CH5 spectrometer. Microanalyses were performed by the Physical-Analytical Service Department of the Schering-Plough Corp.

2,3-Dimethyl-8-phenethylimidazo[1,2-*a*]pyridine (18). A mixture of 4.4 g (0.022 mol) of 2-amino-3-phenethylpyridine[1] and 3.3 g (0.022 mol) of 3-bromobutan-2-one (Eastman) in 80 mL of ethanol was heated under reflux for 20 h. Most of the ethanol was removed by distillation, and the residual material was crystallized from acetonitrile (75 mL) and ether (250 mL). The solid was isolated by filtration and dissolved in 200 mL of 1 N hydrochloric acid. The acidic solution was washed with ethyl acetate (2 × 100 mL). The aqueous solution was adjusted to pH 11.5−12 by the addition of 50% sodium hydroxide. The basic solution was extracted with dichloromethane (3 × 120 mL). The dichloromethane extracts were combined and dried (Na_2SO_4). Following filtration, the dichloromethane was removed under reduced pressure to afford a solid. Recrystallization from isopropyl ether gave 1.0 g (0.004 mol) (18%) of 2,3-dimethyl-8-phenethylimidazo[1,2-*a*]pyridine (**18**), mp 85−88 °C. Anal. ($C_{17}H_{18}N_2$) C, H, N.

2,3-Dimethyl-8-(phenylmethoxy)imidazo[1,2-*a*]pyrazine (19). A mixture of 31.1 g (0.24 mol) of 2-amino-3-chloropyrazine[2] and 36.5 g (0.24 mol) of 3-bromobutan-2-one (Eastman) in 13 mL of ethanol was heated under reflux for 24 h. Upon cooling, the mixture was partitioned between 150 mL of chloroform, 100 mL of water, and 100 mL of 1.1 M sodium bicarbonate. The chloroform layer was separated, and the aqueous solution was extracted with chloroform (2 × 150 mL). The chloroform extracts were combined and dried (Na_2SO_4). Following filtration, the chloroform was removed under reduced pressure to afford a solid. Flash chromatography on silica gel eluting with ethyl acetate gave 8.7 g (0.048 mol) (20%) of 2,3-dimethyl-8-chloroimidazo[1,2-*a*]pyrazine, mp 169.5−172 °C, which was used without further purification.

To a stirred suspension of 1.39 g (0.029 mol) of sodium hydride in mineral oil (50%) in 20 mL of *N*,*N*-dimethylformamide was added a solution of 3.13 g (0.029 mol) of benzyl alcohol in 10 mL of *N*,*N*-dimethylformamide over 5 min, and the mixture was stirred an additional 2 h at room temperature. The mixture was cooled to 5−10 °C, and a solution of 4.79 g (0.026 mol) 2,3-dimethyl-8-chloroimidazo[1,2-*a*]pyrazine in 50 mL of *N*,*N*-dimethylformamide was added dropwise over 0.5 h, followed by 12 h at room temperature. The solvent was removed under reduced pressure, the residue partitioned between dichloromethane and water, and the aqueous layer extracted with dichloromethane. The dichloromethane extracts were combined and dried (Na_2SO_4). Following filtration, the dichloromethane was removed under reduced pressure to give an oil. Trituration and recrystallization from isopropyl ether gave 4.25 g (0.016 mol) (62%) of 2,3-dimethyl-8-(phenylmethoxy)imidazo[1,2-*a*]pyrazine (**19**): mp 104.5−109.5 °C. Anal. ($C_{15}H_{15}N_3O \cdot {}^1/_8H_2O$) C, H, N.

2-(Trifluoromethyl)-3-methyl-8-(phenylmethoxy)imidazo[1,2-*a*]pyridine (20). 2-(Trifluoromethyl)-3-(hydroxymethyl)-8-(phenylmethoxy)imidazo[1,2-*a*]pyridine[1] (54.8 g, 0.17 mol) was suspended in 1.6 L of dichloromethane. To the reaction mixture was 0 °C was added dropwise with stirring 20.2 g (0.17 mol) of thionyl chloride. The solution was stirred for 1 h, and the solid that formed was isolated by filtration, washed thoroughly with dichloromethane, and dried to give 2-(trifluoromethyl)-3-(chloromethyl)-8-(phenylmethoxy)imidazo-[1,2-*a*]pyridine hydrochloride which was used without further purification.

To a suspension of 1.01 g (0.027 mol) of lithium aluminum hydride in 500 mL of tetrahydrofuran at 0 °C was added 5.0 g (0.013 mol) of 2-(trifluoromethyl)-3-(chloromethyl)-8-(phenylmethoxy)imidazo[1,2-*a*]pyridine hydrochloride in portions so the temperature remained below 10 °C. After the mixture was stirred at 0−5 °C for an additional 1 h, 1.5 mL of water was added dropwise at 0−10 °C, followed by 1.5 mL of 15% sodium hydroxide and then 5.0 mL of water. The mixture was allowed to warm to room temperature with stirring, and the solids were removed by filtration. The solids were washed thoroughly with hot tetrahydrofuran (500 mL) and hot chloroform (4 × 250 mL). The filtrate and washings were combined and dried (K_2CO_3). Following filtration, the solvents were removed under reduced pressure to give a solid. HPLC on silica gel eluting with chloroform gave 2.97 g (0.010 mol) (77%) of 2-(trifluoromethyl)-3-methyl-8-(phenylmethoxy)imidazo[1,2-*a*]pyridine (**20**): mp 144.5−145 °C. Anal. ($C_{16}H_{13}F_3N_2O$) C, H, N, F.

References

(1) Kaminski, James J.; Bristol, J. A.; Puchalski, C.; Lovey, R. G.; Elliott, A. J.; Guzik, H.; Solomon, D. M.; Conn, D. J.; Domalski, M. S.; Wong, S. C.; Gold, E. H.; Long, J. F.; Chiu, P. J. S.; Steinberg, M.; McPhail, A. T. Antiulcer Agents 1. Gastric Antisecretory and Cytoprotective Properties of Substituted Imidazo[1,2-*a*]pyridines. *J. Med. Chem.* **1985**, *28*, 876−892.

(2) Kaminski, James J.; Hilbert, J. M.; Pramanik, B. N.; Solomon, D. M.; Conn, D. J.; Rizvi, R. K.; Elliott, A. J.; Guzik, H.; Lovey, R. G.; Domalski, M. S.; Wong, S. C.; Puchalski, C.; Gold, E. H.; Long, J. F.; Chiu, P. J. S.; McPhail, A. T. Antiulcer Agents 2. Gastric Antisecretory, Cytoprotective and Metabolic Properties of Substituted Imidazo[1,2-*a*]pyridines and Analogs. *J. Med. Chem.* **1987**, *30*, 2031−2046.

(3) Kaminski, James J.; Perkins, D. G.; Frantz, J. D.; Solomon, D. M.; Elliott, A. J.; Chiu, P. J. S.; Long, J. F. Antiulcer Agents 3. Structure-Activity-Toxicity Relationships of Substituted Imidazo[1,2-*a*]pyridines and a Related Imidazo[1,2-*a*]pyrazine. *J. Med. Chem.* **1987**, *30*, 2047−2051.

(4) Kaminski, James J.; Puchalski, C.; Solomon, D. M.; Rizvi, R. K.; Conn, D. J.; Elliott, A. J.; Lovey, R. G.; Guzik, H.; Chiu, P. J. S.; Long, J. F.; McPhail, A. T. Antiulcer Agents 4. Conformational Considerations and the Antiulcer Activity of Substituted Imidazo[1,2-*a*]pyridines and Related Analogues. *J. Med. Chem.* **1989**, *32*, 1686−1700.

(5) Briving, C.; Andersson, B.-M.; Nordberg, P.; Wallmark, B. Inhibition of Gastric H^+/K^+-ATPase by Substituted Imidazo[1,2-*a*]pyridines. *Biochim. Biophys. Acta* **1988**, *946*, 185−192 and references cited therein.

(6) Kaminski, James J.; Wallmark, B.; Briving, C.; Andersson, B.-M. Antiulcer Agents 5. Inhibition of the Gastric H^+/K^+-ATPase by Substituted Imidazo[1,2-*a*]pyridines and Related Analogues and its Implication in Modeling the High Affinity Potassium Ion Binding Site of the Gastric Proton Pump Enzyme. *J. Med. Chem.* **1991**, *34*, 533−541.

(7) Cramer, R. D., III; Patterson, D. E.; Bunce, J. D. Comparative Molecular Field Analysis (CoMFA). 1. Effect of Shape on Binding of Steroids to Carrier Proteins. *J. Am. Chem. Soc.* **1988**, *110*, 5959−5967.

(8) Marshall, G. R.; Cramer, R. D., III. Three-Dimensional Structure-Activity Relationships. *Trends Pharmacol. Sci.* **1988**, *9*, 285−289.

(9) Doweyko, A. M. The Hypothetical Active Site Lattice. An Approach to Modeling Active Sites from Data on Inhibitor Molecules. *J. Med. Chem.* **1988**, *31*, 1396−1406.

(10) Doweyko, A. M. New Tool for the Study of Structure Activity Relationships in Three Dimensions. In *Probing Bioactive Mechanisms*; Magee, P., Henry, D. R., Block, J. H., Eds.; ACS Symposium Series 413; American Chemical Society: Washington, DC, 1989; pp 82−104.

(11) Doweyko, A. M. The Hypothetical Active Site Lattice - In Vitro and In Vivo Explorations Using a Three Dimensional QSAR Technique. *J. Math. Chem.* **1991**, *7*, 273−285.

(12) Wiese, M. The Hypothetical Active Site Lattice. In *3D QSAR In Drug Design Theory, Methods and Applications*; Kubinyi, H., Ed.; ESCOM: Leiden, The Netherlands, 1993; pp 431−442.

(13) Saccomani, G.; Stewart, H. B.; Shaw, D.; Lewin, M.; Sachs, G. Characterization of Gastric Mucosal Membranes IX. Fractionation and Purification of K^+-ATPase-Containing Vesicles by Zonal Centrifugation and Free-Flow Electrophoresis Technique. *Biochim. Biophys. Acta* **1977**, *465*, 311−330.

(14) LeBel, D.; Poirier, G. G.; Beaudouin, A. R. A Convenient Method for the ATPase Assay. *Anal. Biochem.* **1978**, *85*, 86−89.

(15) Berglindh, T.; Obrink, K. J. A Method for Preparing Isolated Glands from the Rabbit Gastric Mucosa. *Acta Physiol. Scand.* **1976**, *96*, 150−159.

(16) Bradford, M. M. A Rapid and Sensitive Method for the Quantitation of Microgram Quantities of Protein Utilizing the Principle of Protein-Dye Binding. *Anal. Biochem.* **1976**, *72*, 248−254.

(17) Perrin, D. D.; Dempsey, B.; Serjeant, E. J. *pK_a Prediction for Organic Acids and Bases*; Chapman and Hall: London, England, 1981.

(18) Tripos Associates, 1699 South Hanley Rd., Suite 303, St. Louis, MO 63144.

(19) Still, W. C.; Mohamadi, F.; Richards, N. G. J.; Guida, W. C.; Lipton, M.; Liskamp, R.; Chang, G.; Hendrickson, T.; DeGunst, F.; Hasel, W. MacroModel V1.5, Department of Chemistry, Columbia University, New York, NY 10027.

(20) Hypothesis Software, P.O. Box 237, Long Valley, NJ 07853-0237. HASL Version 3.29 (for PC-compatibles 80387 and higher).

(21) Exographics, P. O. Box 655, West Milford, NJ 07480.

(22) Doweyko, A. M. Three-Dimensional Pharmacophores from Binding Data. *J. Med. Chem.* **1994**, *37*, 1769−1778.

(23) Clark, M.; Cramer, R. D., III; Jones, D. M.; Patterson, D. E.; Simeroth, P. E. Comparative Molecular Field Analysis (CoMFA). 2. Toward its Use with 3 - D Structural Databases. *Tetrahedron Comput. Methodol.* **1990**, *3*, 47−59.

(24) Advanced QSAR Module, Tripos Associates, 1699 South Hanley Rd., Suite 303, St. Louis, MO 63144.

(25) Cho, S. J.; Tropsha, A. Cross-Validated R2 _ Guided Region Selection for Comparative Molecular Field Analysis: A Simple Method to Achieve Consistent Results. *J. Med. Chem.* **1995**, *38*, 1060−1066.

(26) Smith, G. SEA: Steric and Electrostatic Alignment Molecular Superposition Program; QCPE Program No. 567; Department of Chemistry, Indiana University, Bloomington, IN 47405. We thank Dr. John W. Clader of the Schering-Plough Research Institute for porting the code of this program into the UNIX environment.

JM950700S